Superfluidity and phase separation in helium films

A. N. Berker and David R. Nelson
Department of Physics, Harvard University, Cambridge, Massachusetts 02138
(Received 28 September 1978)

A vectorial generalization of the Blume-Emery-Griffiths model is proposed to describe superfluidity in films of ^{3}He-^{4}He mixtures, and is solved by an approximate renormalization scheme due to Migdal. In contrast to bulk mixtures, the line of superfluid transitions is connected to the phase-separation curve by a critical end point. The universal jump of the superfluid density, present in the pure ^{4}He system, is preserved with increasing ^{3}He concentrations x until the critical end point occurs at $x \lesssim 0.12$. At smaller x, phase separation causes a kink in the superfluid density versus temperature curve. No tricritical point occurs for any value of the model parameters, although an effectively tricritical phase diagram is obtained in a certain limit. Lines of constant superfluid density bunch up near the effective tricritical point, as predicted by tricritical scaling theory. This treatment also describes superfluidity in pure ^{4}He films in the presence of two-dimensional liquid-gas phase separation. In addition we calculate the specific heat of the pure ^{4}He system, using the recursion relations of Kosterlitz. This specific heat has a broad maximum above the superfluid transition temperature, corresponding to a gradual dissociation of vortex pairs with increasing temperature.

I. INTRODUCTION AND MODEL HAMILTONIAN

In 1971, Blume, Emery, and Griffiths[1,2] introduced a spin-1 Ising model to simulate the thermodynamics of ^{3}He-^{4}He mixtures along the λ line and at the tricritical point (Fig. 1). Mean-field treatments[1-3] of this model display many features of bulk ^{3}He-^{4}He mixtures, despite the neglect of the continuous rotational symmetry of the degrees of freedom associated with superfluidity. Subsequent work by Riedel and Wegner[4] showed that mean-field theory is in fact correct for tricritical points in all dimensions greater than three. In three dimensions, moreover, the only dependence on the symmetry of the superfluid degrees of freedom is in weak logarithmic corrections to the mean-field predictions.[5] Thus, the success of the Blume-Emery-Griffiths (BEG) model, at least near the tricritical point, is not surprising. Series expansions[6] seem to confirm this general picture.

The BEG model is, however, less appropriate for films of ^{3}He-^{4}He mixtures. Rigorous mathematics[7] rules out conventional superfluidity, namely, a nonzero order parameter, in two-dimensional systems. The "superfluid order parameter" of the BEG model is nevertheless expected to be nonzero even in two dimensions, because of the discrete Ising symmetry. Indeed, Monte Carlo[8] and renormalization-group[9-11] studies of the two-dimensional BEG model yield conventional ordering, although with nonmean-field tricritical exponents.

In this paper, we consider a simple generalization of the BEG model, designed to take into account the continuous rotational symmetry of the superfluid degrees of freedom, and to provide insight into the behavior of films of ^{3}He-^{4}He mixures. BEG used the

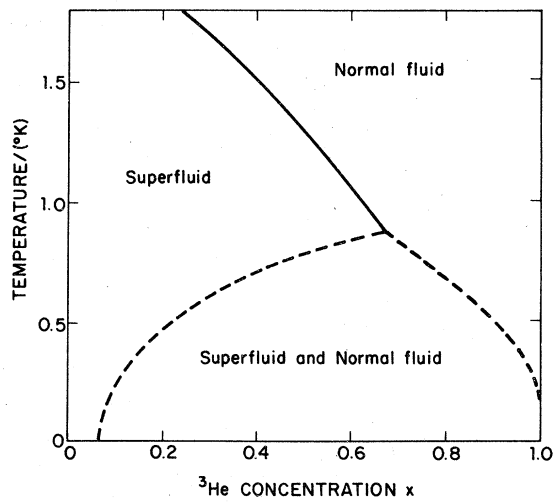

FIG. 1. Tricritical phase diagram of bulk ^{3}He-^{4}He mixtures, from Ref. 32b. The zero-temperature miscibility (coexistence region starts at $x = 0.06$ instead of $x = 0$) is a quantum-mechanical effect.

 ©1979 The American Physical Society

model Hamiltonian

$$-\frac{\mathcal{H}^{\mathrm{BEG}}}{k_B T} = J\sum_{\langle ij\rangle} s_i s_j + K\sum_{\langle ij\rangle} s_i^2 s_j^2 - \Delta\sum_i s_i^2 \ , \qquad (1.1)$$

where the spin s_i is located at the site i of some regular lattice, and assumes the discrete values of 0, ± 1. The first two sums are over nearest-neighbor pairs $\langle ij\rangle$, k_B and T are the Boltzmann constant and the absolute temperature, and the factor $-1/k_B T$ has been absorbed into the coupling constants J, K, and Δ. This can be regarded as a lattice-gas model for mixtures, where the state $s_i = 0$ represents the occupation of site i by a ^{3}He atom, and the states $s_i = \pm 1$ give the superfluid degrees of freedom when site i is occupied by a ^{4}He atom. The generalization of Eq. (1.1) which we have studied in two dimensions is

$$-\frac{\mathcal{H}}{k_B T} = J\sum_{\langle ij\rangle} \vec{s}_i\cdot\vec{s}_j + K\sum_{\langle ij\rangle} |\vec{s}_i|^2|\vec{s}_j|^2 - \Delta\sum_i |\vec{s}_i|^2 \ , \qquad (1.2a)$$

where $\vec{s}_i$ is a two-component vector of length unity or zero, i.e.,

$$\vec{s}_i = (t_i\cos\theta_i \ , \ t_i\sin\theta_i) \ , \qquad (1.2b)$$

with $t_i = 0$, 1 and $0 \leq \theta_i < 2\pi$. Again $\vec{s}_i = 0$ represents occupation by a ^{3}He atom. When site i is occupied by a ^{4}He atom, $\vec{s}_i = (\cos\theta_i, \sin\theta_i)$ reflects the superfluid degrees of freedom, with the appropriate continuous rotational symmetry. Our partition function is

$$Z = \prod_i \left(\sum_{t_i=0}^{1} \int_0^{2\pi} \frac{d\theta_i}{2\pi} \right) e^{-\mathcal{H}/k_B T} \ . \qquad (1.3)$$

The interpretation of the parameters in (1.2a) is as in the BEG model.[1] The bilinear coupling $k_B TJ$ is a potential promoting superfluid ordering. It is related[12] to a bare, areal superfluid density $\rho_0(T)$ by

$$k_B TJ = \hbar^2\rho_0(T)/m^2 \ , \qquad (1.4)$$

where m is the mass of a ^{4}He atom. The biquadratic coupling $k_B TK$ derives from an isotope effect,

$$K = K_{33} + K_{44} - 2K_{34} \ , \qquad (1.5)$$

when each nearest-neighbor $^\alpha$He-$^\beta$He pair is taken to have a classical potential energy $k_B TK_{\alpha\beta}$. The on-site interaction $k_B T\Delta$ is essentially the difference between the chemical potentials μ_3 and μ_4 of ^{3}He and ^{4}He, i.e.,

$$k_B T\Delta = (\mu_3 - \mu_4) + qk_B T(K_{33} - K_{44}) \ , \qquad (1.6)$$

where q is the number of nearest neighbors of a given lattice site. The above is also a model for superfluidity in pure ^{4}He films in the presence of two-dimensional liquid-gas phase separation.[13] Thus, although the remainder of this article employs the terminology of ^{3}He-^{4}He mixtures, the simple reinterpretation as "vacant sites" of "^{3}He occupied sites" immediately yields a description of superfluidity and condensation in the pure ^{4}He films. The quantity $\langle S_i^2\rangle$ can then be interpreted as a normalized density of ^{4}He atoms.

In the very negative Δ limit ($\Delta \to -\infty$), the states with any $\vec{s}_i = 0$ become negligible in the partition function (1.3), and the planar or XY model is obtained. This can be regarded as a model for superfluidity in pure ^{4}He films, with θ_i representing the phase of the superfluid order parameter. Fluctuations in the magnitude of this order parameter are not taken into account.

Studies of the two-dimensional XY model have a controversial history. Wegner[14] found from a spin-wave calculation that, at low temperatures, correlations decay algebraically rather than exponentially. High-temperature series expansions by Stanley[15] pointed to the existence of a phase transition at finite temperature, notwithstanding Mermin and Wagner's rigorous proof[7,16] of the absence of long-range order. A variety of theoretical ideas were subsequently advanced by Berezinskii,[17] Kosterlitz and Thouless,[18] Zittartz,[19] and Luther and Scalapino.[20]

It has become increasingly clear that a simple picture of superfluidity in pure ^{4}He films, due to Kosterlitz and Thouless[18] and to Berezinskii,[17] is substantially correct. One imagines a superfluid state in which long-wavelength phase fluctuations coexist with a dilute gas of bound vortex-antivortex pairs. Although the phase fluctuations prevent true long-range order, correlations decay algebraically, in contrast to the exponential decay in the normal fluid. A transition out of this superfluid state is driven by the dissociation of a finite fraction of the vortex pairs. Kosterlitz,[21] and subsequently José *et al.*,[22] have carried out calculations on the two-dimensional planar model which confirm this picture. One striking consequence of these theories is that, at the transition temperature T_s, the superfluid density $\rho_s(T)$ in a pure ^{4}He film jumps discontinuously to zero in a universal way.[23] Specifically, it is found that one has

$$\lim_{T\to T_s^-} \frac{\rho_s(T)}{T} = \frac{2m^2 k_B}{\pi\hbar^2} = 3.491\times 10^{-9}\frac{\mathrm{g}}{\mathrm{cm}^2\ ^\circ\mathrm{K}} \ , \qquad (1.7)$$

regardless of the film thickness, substrate, etc. This prediction has been confirmed experimentally in third-sound measurements by Rudnick and collaborators,[24] and in Andronikoshvilli type measurements by Bishop and Reppy.[25]

Here, we study how a systematic dilution with ^{3}He atoms[26] affects the results sketched above. We use an approximate renormalization scheme due to Migdal,[27,28] which comes remarkably close to the correct result for the pure system.[22] The types of phase di-

agrams of the dilute system can be anticipated as syntheses of two phenomena: (i) In the pure system, the vortex-unbinding superfluid transition occurs[18,21,22] at a temperature $J^{-1}=J_s^{-1}(x=0)$,

$$J_s^{-1}(x=0)\simeq 1 \ , \tag{1.8}$$

where

$$x=1-\langle s_i^2\rangle \tag{1.9}$$

is the ^{3}He concentration. Dilution weakens the effective coupling between the superfluid degrees of freedom, so the transition should occur at lower temperature, i.e., $J_s^{-1}(x)$ decreases as x is increased from 0. (ii) As the ^{3}He concentration x is increased, one expects a phase separation (into two phases, one rich in ^{3}He, the other in ^{4}He) at temperatures below a critical temperature

$$(J+K)_c^{-1}\sim 1 \ . \tag{1.10}$$

Clearly, the temperature-concentration phase diagrams of our model will strongly depend on K/J.

For $K/J \gg 1$, the phase separation curve towers over the superfluid transition at $x=0$. The only readily conceivable phase diagram is shown in Fig. 2. The superfluid transition temperature decreases with increasing x, until it joins the coexistence curve at a critical end point. No multicritical phenomena (such as new exponents) occur at an end point, which is just the point where a higher-order transition gets pre-empted by a first-order line. Such behavior could be expected in, for example, ^{4}He-Ne mixtures, since the "isotope effect" should be rather large in that case.

For $K/J \ll 1$, on the other hand, another possibility is shown in Fig. 1. The line of superfluid transitions drops down to join the coexistence curve at its tip. This tip is then a tricritical point, which has its own distinctive set of exponents, as evidenced, for example, by the different shapes of the coexistence curves in Figs. 1 and 2. This is the case for bulk ^{3}He-^{4}He mixtures (to which Fig. 1 applies), which shows that the isotope effect is weak compared with the superfluid coupling.

Both types[29] of phase diagrams have been found in the mean-field[1,3] and renormalization-group[9] investigations of the BEG model. The Migdal renormalization scheme which we use has, in fact, yielded both types of phase diagrams for another two-dimensional system.[30]

In a given physical situation, as temperature is increased, the Hamiltonian parameters J and K decrease, because an inverse temperature was absorbed into them [Eq. (1.2a)]. But their ratio K/J is mainly unchanged, and determined by film thickness, substrate, etc. This ratio may vary significantly with film thickness. As the thickness is reduced from large values to one or two layers, fluctuations should be more effective in reducing the pure superfluid transi-

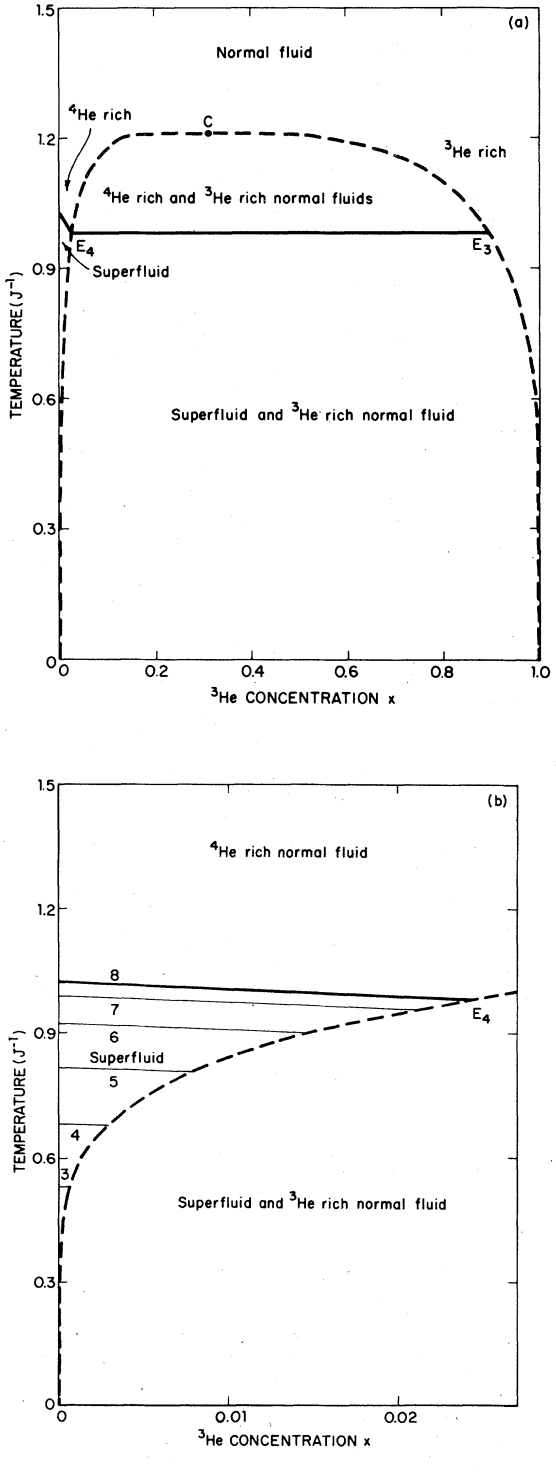

FIG. 2. End-point phase diagram of the vectorialized BEG model at $K/J=1$. The dark, full lines indicate higher-order superfluid phase transitions. In (b), constant $\rho_s(T)/k_BT$ curves are drawn with light, full lines: Curve n corresponds to $\rho_s(T)/k_BT=16\,m^2/n\pi\hbar^2$.

tion temperature than in diminishing the Ising phase separation T_c. Since these characteristic temperatures are determined by Eqs. (1.8) and (1.10) in our model, K/J should increase with decreasing film thickness. It would be rather large for thin films.

The results of our renormalization-group treatment of the vectorialized BEG model (1.2) in two dimensions (on a triangular lattice, which is the close-packing lattice of two dimensions) are summarized as follows. In the space of J^{-1}, K/J, and Δ, a first-order surface of concentration discontinuities separates ^{3}He-rich and ^{4}He-rich phases. This surface terminates in a line of Ising-type critical points. The ^{4}He-rich portion of the phase diagram is further divided into superfluid and normal fluid phases by a surface of superfluid phase transitions. The universal jump[23] in the superfluid density, present in the pure system, is preserved at this surface. Our renormalization procedure yields the correlation-length critical exponent $\nu = \infty$ for these superfluid transitions, in agreement with previous theory.[22] The surface of superfluid transitions terminates in a line of critical end points on the first-order surface.

Our temperature-concentration phase diagrams, for large K/J, are distinctly of the end-point type, as shown in Fig. 2 for $K/J = 1$. As K/J is decreased, the end point slides up the coexistence curve, but never actually reaches the phase-separation critical point at the tip. Thus, *there is never a tricritical point.* The shape of the coexistence curve is always determined by the Ising critical[31] exponent $\beta = \frac{1}{8}$, rather than by some new tricritical phase-separation exponent. As T approaches the phase-separation critical temperature T_c from below, the coexisting ^{3}He concentrations $x_\pm(T)$ merge as

$$x_+(T) - x_-(T) \sim (T_c - T)^{1/8} \ . \qquad (1.11)$$

This very flat behavior should be contrasted with that observed in bulk mixtures, where $x_\pm(T)$ approach each other linearly[32] in T. As K/J tends to zero, however, the end point comes very close to the phase-separation critical point. For example, Fig. 3 shows $K/J = 0$, the Blume-Capel[2] limit. The end point occurs at $J^{-1} = 0.6581$, whereas the phase-separation critical point is at $J^{-1} = 0.6615$. The overall phase diagram in Fig. 3 does resemble a tricritical phase diagram. In this case, lines of constant $\rho_s(T)/k_B T$ bunch up as they approach the "effective tricritical point" (formed by the closely situated end point and critical point), as predicted by tricritical scaling theory (Sec. II B).

For any given fixed K/J, we find that the line of superfluid phase transitions of the type encountered in pure ^{4}He films, namely, the transition line $T_s(x)$ stretching from $x = 0$, is rather short. The first-order

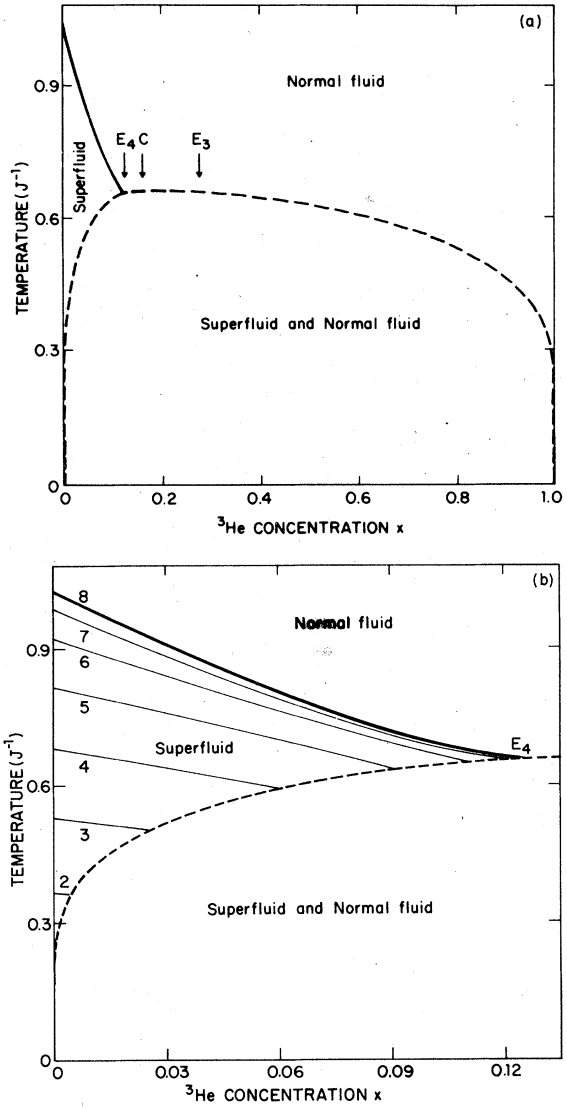

FIG. 3. Effectively tricritical phase diagram of the vectorialized BEG model at the Blume-Capel plane ($K = 0$). The dark, full lines indicate higher-order superfluid phase transitions. In (b), constant $\rho_s(T)/k_B T$ curves are drawn with light, full lines: Curve n corresponds to $\rho_s(T)/k_B T = 16\, m^2/n\pi\hbar^2$.

transition pre-empts it at 12% of ^{3}He or less, at the critical end point. The ^{3}He concentration at the end point is the maximum amount of ^{3}He which can be included into a superfluid domain. This limit concentration decreases with increasing K/J, being equal to 0.12 for $K/J = 0$, and equal to 0.02 for $K/J = 1$. These values are quite different from the limit concentration $x = 0.67$ of bulk mixtures,[32] which is that of the tricritical point. This difference can be under-

stood qualitatively, by noting that a lesser amount of impurity is needed to drastically weaken the connectivity of interacting superfluid degrees of freedom, when these are arrayed in a lower-dimensional space.

For higher ^{3}He concentrations, the onset of superfluidity in films becomes *nonuniversal,* because of phase separation. As this concentration x is increased from its end-point value, the transition discontinuity in $\rho_s(T)/k_BT$ decreases, but is still finite. This happens in the density interval ($0.12 < x < 0.27$ for $K/J = 0$) where phase separation occurs at temperatures higher than the end-point temperature, so that phase separation is initially into a ^{3}He-rich phase and a ^{4}He-rich normal fluid. The latter undergoes the superfluid transition when the system is further cooled to the end-point temperature. At higher ^{3}He concentrations, the phase-separation temperature is below the end-point temperature, so that the ^{4}He-rich phase is always superfluid. In this range, $\rho_s(T)/k_BT$ increases linearly from zero as superfluidity appears at phase separation. Representative superfluid density versus temperature curves are given in Fig. 4. At low ^{3}He concentrations, where the film undergoes the universal[23] superfluid transition, phase separation occurs at a lower temperature. This causes a *kink* in the superfluid density curve (point P in Fig. 4).

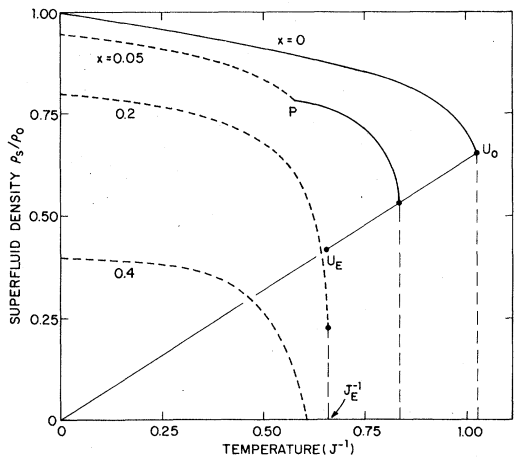

FIG. 4. Superfluid density fraction ρ_s/ρ_0 as a function of temperature (J^{-1}) at various ^{3}He concentrations x, for $K/J = 0$. The four types of curve (Sec. III) are represented. Dark dashes indicate that phase separation has occurred. This introduces the kink at point P. Discontinuities at the superfluid transition are shown with light dashes. The locus of minimum superfluidity consists of the universally sloped line segment U_0U_E, the vertical segment at the end-point temperature J_E^{-1}, and the $\rho_s/\rho_0 = 0$ axis between J_E^{-1} and zero temperature.

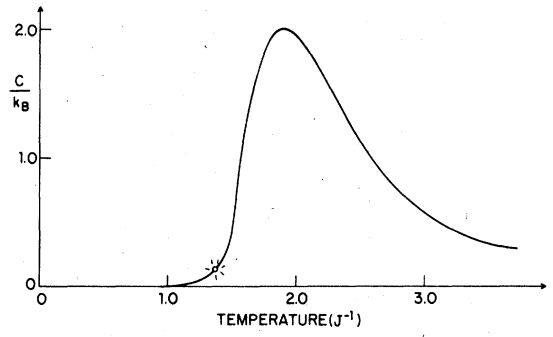

FIG. 5. Vortex contribution to the specific heat of a pure XY model in two demensions. The coupling J is the ratio of the nearest-neighbor interaction energy to $-k_BT$. The circle marks the phase transition temperature, where vortex unbinding first occurs. The specific heat has an unobservable essential singularity at this point.

Specific-heat measurements at fixed concentration would reveal any phase separation by a steplike discontinuity. However, such measurements are not a good probe for superfluidity in films. Indeed, one expects[21] only an unobservably weak essential singularity in the specific heat across the superfluid transition. This question is further explored in the Appendix, where the vortex part of the specific heat of the pure XY model is determined. As seen in Fig. 5, this specific heat rises to a maximum at a temperature higher than the superfluid transition temperature T_s, with no detectable singularity at T_s. The maximum is caused by the gradual dissociation of vortex pairs, beginning at T_s. Pairs separated by shorter and shorter distances become unbound with increasing temperatures, until the average separation of bound pairs becomes of the order of magnitude of the vortex core size. The precise shape, height, and position of the maximum is nonuniversal.

Our present model is applicable to films with several atomic layers, provided one deals with quantities averaged over the film thickness. This averaging is especially simple when the correlation length exceeds the film thickness. However, calculations reported here do not take into account any possibly important effect of a concentration gradient (or even phase separation) perpendicular to the film.[33] The Van der Waals attraction to the substrate is the same for ^{3}He and ^{4}He atoms, but the smaller mass and larger zero-point motion of the ^{3}He atoms should cause them to move preferentially to the surface of a thick film. If experiments show that this is of consequence, our model could be further developed by considering 2 two-dimensional lattices stacked on top of each other, with different chemical potentials (i.e., different on-site interactions Δ) at each layer.[34] In thin-film experiments, it is believed[26] that before any

superfluidity appears, about one layer of atoms "solidifies" on the substrate. Superfluidity is attributed to subsequent layers. Thus, we can reasonably hope that, in any case, our present calculation is applicable when about one layer is added beyond the solidification layer. It is hard to imagine important vertical differentiation in an effectively single atomic-layer fluid.

The remainder of this paper is organized in the following way: In Sec. II, the renormalization procedure is given. It is argued that $\rho_s(T)/k_BT$ is invariant under this renormalization. Then, starting with the special limits of the pure XY model, the asymptotic first-order region, and the spin-$\frac{1}{2}$ Ising model, the global Hamiltonian flows are described. In Sec. III, the resulting phase diagrams and, at fixed ^{3}He concentrations, the temperature dependence of the superfluid density are discussed. The details of the specific-heat calculations are relegated to the Appendix.

II. RENORMALIZATION PROCEDURE AND HAMILTONIAN FLOWS

A remarkably simple and powerful method for obtaining recursion relations for complicated systems in low dimensions has been devised by Migdal.[27] In this section we apply Migdal's method, in a form due to Kadanoff.[28]

A. Recursion relations

Consider a slightly more general form of the Hamiltonian (1.2a), namely,

$$-\frac{\mathcal{H}}{k_BT}=\sum_{\langle ij\rangle} t_it_jV(\theta_i-\theta_j) + K\sum_{\langle ij\rangle} t_it_j-\Delta\sum_i t_i \ , \tag{2.1}$$

where $V(\theta)$ is a periodic function with period 2π. Although upon setting

$$V(\theta)=J\cos\theta \tag{2.2}$$

we recover Eq. (1.2a), the specific form (2.2) is not conserved by the renormalization procedure. Therefore, we have to construct recursion relations for the more general form (2.1). Equation (2.2) is used as initial condition, from which originate the Hamiltonian flows induced by renormalization, in the larger parameter space of Eq. (2.1). (Similarly, if one were solely interested in a system with no biquadratic coupling, $K=0$, the renormalization procedure would generate nonzero K, which would then have to be included into the analysis.)

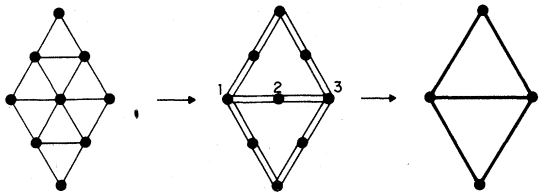

FIG. 6. Migdal transformation for the triangular lattice (Sec. II A).

Any renormalization procedure is based on the elimination of a subset of the degrees of freedom inside the partition sum. With our partition sum (1.3), this could be quite a problem. Progress is made, however, by first moving some of the interaction bonds as shown in Fig. 6. One then integrates without difficulty over the isolated one-dimensional degrees of freedom, obtaining effective interactions between the remaining degrees of freedom. The justification of the bond-moving approximation was discussed by Kadanoff.[28] We recall here that this approximation obeys a lower-bound variational principle for the free energy.[35] It is known to be fairly accurate at lower critical dimensionalities, which is the case for the XY degrees of freedom in Eq. (2.1). Figure 6 shows the adaptation of bond moving to the triangular lattice, previously used in the study of epitaxial ordering in physisorbed films.[30]

The bond-moving prescription is completed by considering the treatment of the on-site interactions. One has to decide what fraction of these gets moved with the nearby bonds. For this, a scheme introduced by Emery and Swendsen[36] is employed. The Hamiltonian (2.1) is rewritten

$$-\frac{\mathcal{H}}{k_BT}=\sum_{\langle ij\rangle} t_it_j[V(\theta_i-\theta_j)-V(0)]-\tfrac{1}{2}[K+V(0)] \times\sum_{\langle ij\rangle}(t_i-t_j)^2-\{\Delta-\tfrac{1}{2}q[K+V(0)]\}\sum_i t_i \ . \tag{2.3}$$

The first two terms are regarded as bonds, to be moved in their entirety. The last term is regarded as truly on-site, and is not moved. The effect of bond moving should be small at high temperatures, because the moved entities go to zero with $V(\theta)$, $K\sim 1/k_BT\to 0$. At low temperatures, the effect of this bond moving should again be small, this time because the configurations with $t_i=t_j$, $\theta_i\simeq\theta_j$ dominate, and the local operators inside the moved entities vanish for these configurations.[36] Finally, note that when we have $V(\theta)=K=0$, nothing is moved. This means that, along the entire Δ axis, the partition function is evaluated exactly. This axis acts as an "anchor" to the approximate evaluations in full J, K, and Δ space. These aspects of the Emery-Swendsen

scheme are certainly expected to mitigate the approximation inherent in bond moving.

The procedure described above has been carried out for a triangular lattice. Starting with a Hamiltonian of the form (2.1), we obtain a new Hamiltonian of the same form, coupling the thinned-out degrees of freedom. In terms of

$$u(\theta) \equiv e^{V(\theta)-V(0)}, \quad w \equiv e^{-K-V(0)}, \quad \text{and } z \equiv e^{\Delta} , \tag{2.4}$$

the parameters of the new Hamiltonian (primed) are given by the simple recursion relations

$$u'(\theta) = \frac{w^5 z + \int_0^{2\pi} \frac{d\phi}{2\pi} u^2(\phi) u^2(\theta-\phi)}{w^5 z + A_4} , \tag{2.5a}$$

$$w' = \frac{(w^3 z + A_2)^2}{(wz+1)(w^5 z + A_4)} , \tag{2.5b}$$

$$z' = w^9 z \frac{(wz+1)^6}{(w^3 z + A_2)^6} , \tag{2.5c}$$

where

$$A_n \equiv \int_0^{2\pi} \frac{d\phi}{2\pi} u^n(\phi) . \tag{2.5d}$$

It is computationally convenient to follow the recursion of the Fourier components F of $u(\theta)$, i.e.,

$$F\{u(\theta)\} \equiv f(s) = \int_0^{2\pi} \frac{d\theta}{2\pi} e^{is\theta} u(\theta) ,$$

$$u(\theta) = \sum_{s=-\infty}^{\infty} e^{-is\theta} f(s) . \tag{2.6}$$

Sums instead of integrals are to be evaluated when

$$f'(s \neq 0) = g^2(s)/(w^5 z + A_4) , \tag{2.7a}$$

$$g(s) = F\{u^2(\theta)\} = \sum_{p=-\infty}^{\infty} f(p) f(s-p) \tag{2.7b}$$

are used instead of Eq. (2.5a). The $s=0$ component can be evaluated from the normalization condition

$$1 = u'(\theta=0) = \sum_{s=-\infty}^{\infty} f'(s) . \tag{2.8}$$

Also, $f(-s) = f(s)$ is conserved, and Eq. (2.5d) is evaluated as

$$A_2 = g(s=0), \quad A_4 = \sum_{s=-\infty}^{\infty} g^2(s) . \tag{2.9}$$

For the present problem, it was sufficient to keep the $|s| \leq 10$ components, setting to zero the higher ones (which were of negligible magnitude) in order to truncate the infinite sums. However, we did perform spot checks with up to $|s| \leq 40$ nonzero.

B. Invariance of the superfluid density

In 1966, Josephson[37] argued that the superfluid density in bulk helium near the lambda point would behave as

$$\rho_s(T) \sim (T_\lambda - T)^\nu , \tag{2.10}$$

where $\nu \simeq \frac{2}{3}$ is the correlation-length exponent. In d dimensions, this result (which is a consequence of the rotational invariance of the superfluid) reads[38]

$$\rho_s \sim \xi_T^{2-d} , \tag{2.11}$$

where ξ_T is the correlation length describing the decay of correlations transverse to the order parameter. If $\{K_\alpha\}$ denotes a set of Hamiltonian parameters on which ρ_s can depend, the restatement of the Josephson relation in renormalization-group context is[39]

$$\rho_s(\{K_\alpha\}) = e^{(2-d)l} \rho_s(\{K_\alpha(l)\}) , \tag{2.12}$$

where $e^l = b$ is the Kadanoff block size and $\{K_\alpha(l)\}$ are the rescaled parameters. Although the derivation of Eq. (2.12) relies on the existence of long-range order,[38,39] it does suggest that ρ_s is invariant under a renormalization transformation in precisely $d=2$.

To explore this question with the vectorialized BEG model, let us introduce a superfluid velocity field

$$\vec{v}_{ij} = (\hbar/ma)(\theta_i - \theta_j)\vec{\delta}_{ij} , \tag{2.13}$$

where i and j are two nearest-neighbor sites, a is the distance between them, and m is the mass of a ^{4}He atom. The velocity (2.13) points along the unit bond-vector $\vec{\delta}_{ij}$. A two-dimensional superfluid density can now be defined in terms of the correlations of the velocity field,[40,41]

$$\frac{k_B T}{\rho_s} = \frac{2a^2}{qN} \left\langle \sum_{\langle ij \rangle} \vec{v}_{ij} \cdot \sum_{\langle kl \rangle} \vec{v}_{kl} \right\rangle , \tag{2.14}$$

where each sum is over all nearest-neighbor bonds, $\frac{1}{2}qN$ is the number of such bonds, and N is the number of sites.

As discussed by Kadanoff,[28] ambiguities arise when Migdal's decimation is used to evaluate correlations such as Eq. (2.14). A heuristic argument can, however, be constructed for the invariance of $\rho_s/k_B T$ under the Migdal procedure in two dimensions. Consider a transformation which first "moves" the bond velocities in Eq. (2.14) together with the bond interactions. For the generalization[30] of the transformation shown in Fig. 6 to block size b, one obtains velocities in Eq. (2.14) which are b times the starting Eq. (2.13), i.e.,

$$\vec{v}_{ij} \to b\, \vec{v}_{ij} . \tag{2.15}$$

The terms in each velocity sum of Eq. (2.14) are now simply grouped into subsums $b\vec{v}_{ij}+b\vec{v}_{jk}+\cdots+b\vec{v}_{pr}$ along lines connecting two sites (i and r) which will remain after the renormalization. These linear subsums are immediately performed. For example, for the sites labeled 1, 2, and 3 in Fig. 6, this proceeds as

$$b\vec{v}_{12}+b\vec{v}_{23}=b\frac{\hbar}{ma}(\theta_1-\theta_3)\vec{\delta}_{13}\equiv b^2\vec{v}'_{13} \ , \quad (2.16)$$

where we recall that the transformed nearest-neighbor distance is $a'=ba$. Dedecorating all the isolated sites such as site 2, Eq. (2.14) becomes

$$\frac{k_BT}{\rho_s}=\frac{2(ba)^2}{q(b^{-2}N)}\left\langle\sum_{\langle ij\rangle}\vec{v}'_{ij}\cdot\sum_{\langle kl\rangle}\vec{v}'_{kl}\right\rangle' \ , \quad (2.17)$$

where each sum is over all nearest-neighbor bonds of the transformed system, and the thermal average is evaluated using the transformed Hamiltonian. Since we have $a'=ba$ and $N'=b^{-2}N$, the right-hand side of Eq. (2.17) is just k_BT'/ρ_s'. Thus, the lattice analogue of Eq. (2.12), for our generalized BEG model in two dimensions, is obtained. Writing ρ_s/k_BT as a functional of $V(\theta)$, K, and Δ, we have

$$\frac{\rho_s}{k_BT}\{V(\theta),K,\Delta\}=\frac{\rho_s}{k_BT}\{V'(\theta),K',\Delta'\} \ . \quad (2.18)$$

The superfluid density, normalized by absolute temperature, is indeed left unchanged by the Migdal transformation in two dimensions.

According to the above argument, renormalization-group trajectories are also lines of constant ρ_s/k_BT. This invariance property can be used to obtain superfluid densities,[23] provided that Hamiltonians eventually interate into regions where Eq. (2.14) is easily evaluated. As discussed in Sec. II E, in the present calculation, Hamiltonians of the superfluid phase iterate onto the Villain model[42] line of fixed points. Equation (2.14) is then readily evaluated by extending the angle integrations to $\pm\infty$, yielding

$$(\rho_s/k_BT)\simeq(m^2/\hbar^2)J_v \ , \quad (2.19)$$

where J_v parametrizes the Villain model as in Eq. (2.25). This result, used in conjunction with Eq. (2.18), produced the lines of constant ρ_s/k_BT in the phase diagrams of Figs. 2, 3, 7, and 8, and the superfluid density curves of Fig. 4.

The invariance of ρ_s/k_BT would have interesting consequences near a tricritical point, should one actually exist. In that case, ρ_s/k_BT would become a function of just two relevant thermodynamic fields, say K_1 and K_2. The phenomenological[43] and renormalization-group[4] formulations of tricritical scaling would then assert that

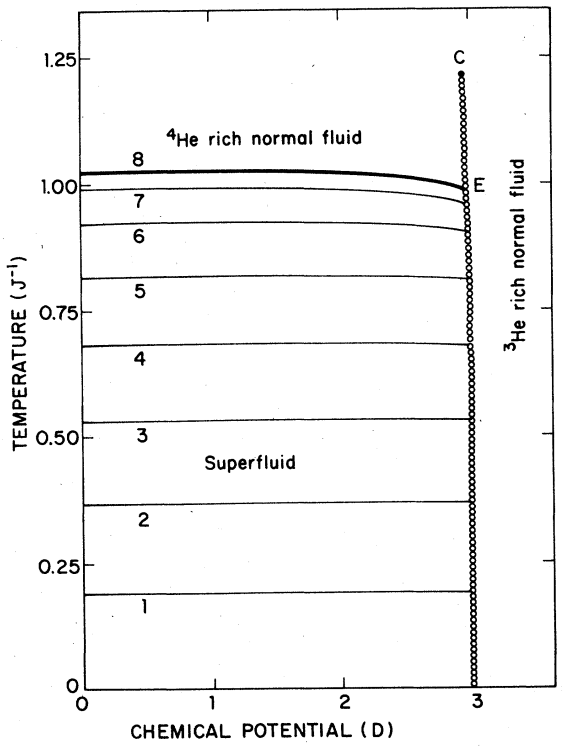

FIG. 7. End-point phase diagram of the vectorialized BEG model at $K/J=1$. The dark, full line and the line of open circles (ooo) respectively indicate higher-order and first-order transitions. The dark circle (●) marks the isolated critical point, and E labels the critical end point. Constant $\rho_s(T)/k_BT$ curves are drawn with light, full lines: Curve n corresponds to $\rho_s(T)/k_BT=16\,m^2/n\pi\hbar^2$.

$$\frac{\rho_s}{k_BT}(K_1,K_2)=\frac{\rho_s}{k_BT}(b^{\lambda_1}K_1,b^{\lambda_2}K_2) \ , \quad (2.20)$$

where $K_1=K_2=0$ corresponds to the tricritical point. This implies that ρ_s/k_BT is a function of only K_1/K_2^{ϕ}, with $\phi=\lambda_2/\lambda_1$, i.e.,

$$\frac{\rho_s}{k_BT}(K_1,K_2)=R\left(\frac{K_1}{K_2^{\phi}}\right) \ . \quad (2.21)$$

We are led to the conclusion that the finite limiting value of ρ_s/k_BT at the tricritical point is indeterminate, depending instead on the path of approach! Lines of constant ρ_s/k_BT converge onto the tricritical point. Although we found no tricritical fixed point in our calculation, this convergence is exhibited at the scale of Fig. 8(a). The constant ρ_s/k_BT curves labeled 8 through 5 apparently meet at point T_e, and have ρ_s/k_BT values of $2m^2/\pi\hbar^2$ through $(3.2)m^2/\pi\hbar^2$.

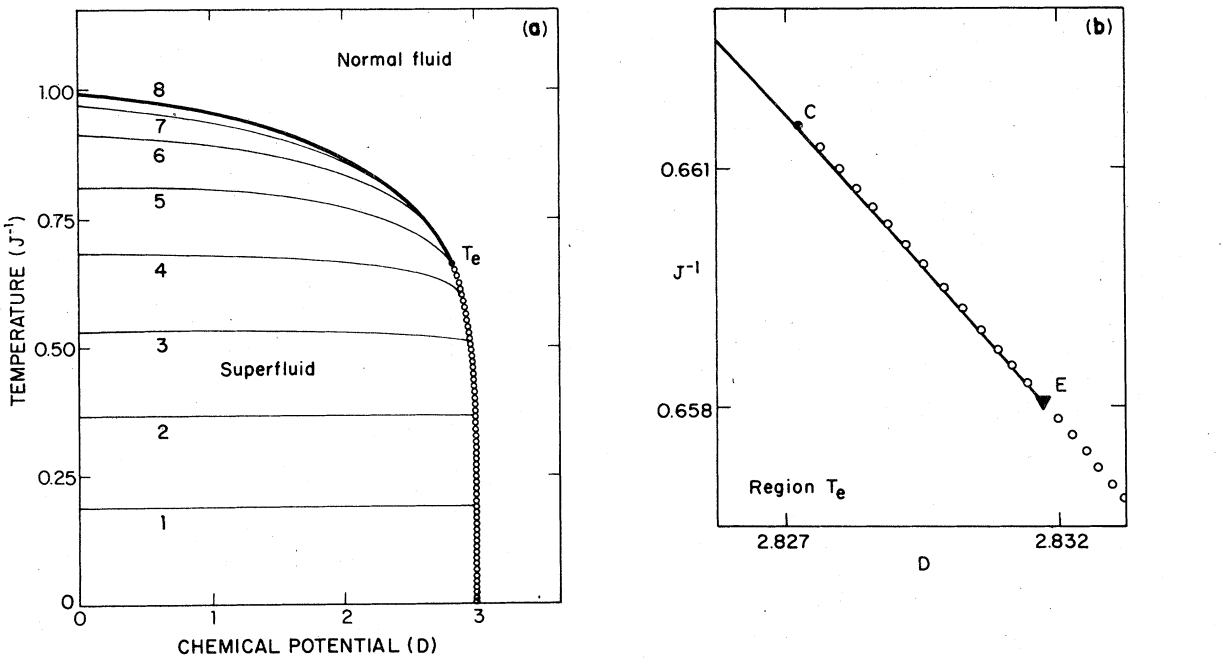

FIG. 8. (a) Effectively tricritical phase diagram of the vectorialized BEG model at the Blume-Capel plane ($K=0$). The dark, full line and the line of open circles (ooo) respectively indicate higher-order and first-order transitions. At the scale of this figure, these lines meet at the effective tricritical point T_e. Constant $\rho_s(T)/k_BT$ curves are drawn with light, full lines: Curve n corresponds to $\rho_s(T)/k_BT = 16\,m^2/n\pi\hbar^2$. As predicted by tricritical scaling theory (Sec. II B), curves 5–8 apparently converge onto the effective tricritical point. (b) Detailed view of the region T_e. [In going from (a) to (b), the horizontal and vertical scales were respectively blown up by factors of 333 and 125, so that (b) actually covers less area than the black point at T_e in (a).] The end-point structure is seen here: (●) and(▼) respectively mark the critical point terminating the first-order line and the end point terminating the higher-order line.

C. Pure XY limit

For $\Delta \to -\infty$, from Eq. (2.5a) we recover Migdal's recursion relation[27] for the generalized XY Hamiltonian

$$-\frac{\mathcal{H}^{XY}}{k_BT} = \sum_{\langle ij\rangle} [V(\theta_i-\theta_j) - V(0)] \ , \tag{2.22}$$

namely,

$$u'(\theta) = A_4^{-1} \int_0^{2\pi} \frac{d\phi}{2\pi}\, u^2(\phi)\, u^2(\theta-\phi) \ , \tag{2.23}$$

or in terms of Fourier components

$$f'(s) = A_4^{-1} \left[\sum_{p=-\infty}^{\infty} f(p) f(s-p) \right]^2 . \tag{2.24}$$

This recursion relation was studied in some detail by Migdal[27] and by José *et al.*[22] As discussed in detail by the latter authors, a low temperature, but otherwise arbitrary $V(\theta)$, relaxes after a few iterations to a Villain potential[42] with Fourier components

$$f_v^*(s) = e^{-s^2/2J_v} \left[\sum_{p=-\infty}^{\infty} e^{-p^2/2J_v} \right]^{-1} . \tag{2.25}$$

Here again, the coupling constant J_v should be thought of as an inverse temperature.

At low temperatures, the Villain potential (2.25) is very nearly invariant under the renormalization procedure, as can be checked by substituting Eq. (2.25) into Eq. (2.24), and approximating the sums by integrals. In fact, a "quasifixed line" of functions of the form (2.25) is found numerically[22,27] for $J_v^{-1} \lesssim \frac{1}{2}\pi$. Unfortunately, a small drift toward high temperature is always present, so that all finite-temperature initial conditions eventually reach an infinite-temperature fixed point at $V(\theta)=0$. However, for example, an initial potential (2.25) with $J_v^{-1} = \frac{3}{2}(\frac{1}{2}\pi)$ takes 11 iterations to reach $V(\theta) \sim 10^{-38}$, whereas over 12,000 iterations are necessary for an initial $J_v^{-1} = \frac{1}{2}(\frac{1}{2}\pi)$. For still lower temperatures, Eq. (2.25) is numerically indistinguishable from a fixed point. Since more rigorous treatments[21,22] of the XY model do produce genuine fixed-line behavior terminating at $J_v^{-1} \simeq \frac{1}{2}\pi$; the drift here must be regarded as a defect of Migdal's renormalization procedure. In this work, we effectively ignore this small drift toward high temperature, and consider

$$f(s)=f_\nu^*(s),\quad J_\nu^{-1}\leq\tfrac{1}{2}\pi,\quad \Delta\to-\infty \qquad (2.26)$$

to be a line segment of fixed points (S_0S_1 in Fig. 9). The initial coupling given in Eq. (2.2), namely, $V(\theta)=J\cos\theta$, maps onto this fixed line for $J^{-1}\leq 1.025$.

Finally, in this $\Delta\to-\infty$ limit, states with any $t_i=0$ are negligible in the partition sum (1.3), and the biquadratic coupling K becomes an additive constant in the Hamiltonian. Concurrently, its recursion relation (2.5b) is slaved to $V(\theta)$, i.e.,

$$w'=A_2^2/A_4\ . \qquad (2.27)$$

On the other hand, the coupling Δ has a crucial role: its renormalization determines the stability of the

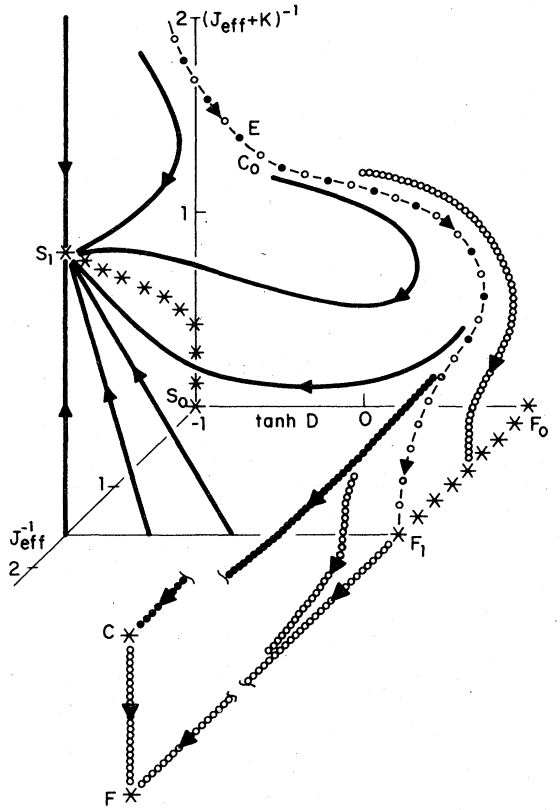

FIG. 9. Global Hamiltonian flows, schematically shown (Sec. II E). Flows through higher-order superfluid transitions, first-order transitions, and Ising-type critical points are respectively indicated by dark full lines, lines of open circles (ooo), and a line of dark circles (●●●). The flow drawn with alternating dashes and open circles (o–o) is through critical end points. The flow drawn with alternating dashes, open and dark circles (o–●–o) is where the Ising-type critical points and the end points come very close together to form effective tricritical points. Fixed points and fixed lines are indicated by (•). The paramagnetic fixed line is not shown.

$\Delta\to-\infty$ limit. The recursion relation (2.5c) reduces to

$$e^{\Delta'}=z'=w^9zA_2^{-6}\ . \qquad (2.28)$$

At the fixed line (2.26), we can substitute Eq. (2.27) into Eq. (2.28) to obtain

$$z'/z=A_2^{12}A_4^{-9}\ . \qquad (2.29)$$

Evaluating A_n for the Villain potential (2.25), approximating sums by integrals we have

$$\frac{z'}{z}=\left(\frac{2}{\pi}\frac{1}{J_\nu}\right)^{3/2}\ . \qquad (2.30)$$

Thus, the $\Delta\to-\infty$ limit is stable at the fixed-line segment (2.26), which is therefore expected to be important in the global phase diagram of the dilute system. From this calculation, we have $\Delta'=\Delta$ at exactly $J_\nu^{-1}=\frac{1}{2}\pi$, so the chemical potential becomes a marginal variable, and the pure XY limit reverses stability at exactly the edge of the fixed-line segment (2.26). At $J_\nu^{-1}>\frac{1}{2}\pi$, Δ is renormalized to less negative values. The above is also precisely the stability behavior of the vortex-core energy $\ln y$ which arises in analytic treatments of the pure XY model.[21,22] Indeed, one would expect ^{3}He atoms to cluster around vortex cores, thus contributing to the core energy.

D. First-order fixed line and Ising behavior

In the limit $\frac{1}{2}qK\sim\Delta\to\infty$, the pure XY recursion relation (2.23) is again recovered, and the preceding discussion applies. A new fixed-line segment (F_0F_1 in Fig. 9) is located at

$$f(s)=f_\nu^*(s),\quad J_\nu^{-1}\leq\tfrac{1}{2}\pi\ , \qquad (2.31a)$$

$$\Delta\to\infty\ , \qquad (2.31b)$$

$$\tfrac{1}{2}qK-\Delta-\ln A_4=0\ , \qquad (2.31c)$$

where A_4 is evaluated by substituting into Eq. (2.9) the Villain potential (2.25), and is approximately $(8\pi J_\nu)^{-1/2}$. This fixed-line segment has one stable direction, $\Delta'\simeq 2\Delta\to\infty$, and one unstable direction involving Eq. (2.31c). For small deviations from zero we have

$$\tfrac{1}{2}qK'-\Delta'-\ln A_4=b^d(\tfrac{1}{2}qK-\Delta-\ln A_4)\ , \qquad (2.32)$$

where $b=2$ is the length rescaling factor and $d=2$ is the lattice dimensionality. Equation (2.32) is a necessary condition for a fixed point whose domain of attraction is a locus of first-order phase transitions, as noted by Nauenberg and Nienhuis.[44] Indeed, our density calculations reveal in the present case a locus of discontinuities in concentration.

These first-order phase transitions can be located also by noting, in the $(\frac{1}{2}q)K \sim \Delta \to \infty$ limit, the crossing of the energies of the two dominant configurations, $\{\vec{s}_i = \vec{s}_j = \ldots = \vec{s}_N \neq 0\}$ and $\{\vec{s}_i = \vec{s}_j = \ldots = \vec{s}_N = 0\}$. This exercise would immediately yield the coefficient $\frac{1}{2}q$ in Eq. (2.31c). The logarithmic correction ln A_4 is a bit more subtle. It derives from the fact that the former configuration (aligned nonzero spins) actually has zero weight in the partition sum, but occurs together with a continuum of spin-wave configurations with infinitesimal energy variations. This logarithmic term does not appear in the original BEG model, which has only discrete excitations. For the present vectorialized model, a renormalization procedure which equipartitions[22] the on-site interactions onto the bonds, in contrast to the Emery-Swendsen scheme,[36] gives the same logarithmic term.

As the coupling between the XY degrees of freedom, e.g., J_v in Eq. (2.25) or J in Eq. (2.2), is weakened, the fixed-line segment (2.31) becomes unstable to the isolated first-order fixed point (F in Fig. 9)

$$V(\theta) = 0, \quad \text{i.e.,} \quad f(s) = \delta_{s0} \ , \tag{2.33a}$$

$$\Delta \to \infty \ , \tag{2.33b}$$

$$\tfrac{1}{2}qK - \Delta = 0 \ . \tag{2.33c}$$

Equation (2.33b) is again stable, $\Delta' \simeq 2\Delta$, and deviations from Eq. (2.33c) again satisfy the Nauenberg-Nienhuis condition.[44] $V(\theta) = 0$ is completely stable. This fixed point occurs in the region $V(\theta) = 0$ where the BEG model reduces[45] to a spin-$\frac{1}{2}$ Ising model. Defining a new variable[45]

$$\sigma_i \equiv 2t_i - 1 \ , \tag{2.34}$$

the $V(\theta) = 0$ Hamiltonian (2.1) becomes

$$-\frac{\mathcal{H}'}{k_B T} = \frac{K}{4}\sum_{\langle ij \rangle}\sigma_i\sigma_j + \tfrac{1}{2}(\tfrac{1}{2}qK - \Delta)\sum_i \sigma_i \ ,$$

$$\sigma_i = \pm 1 \ . \tag{2.35}$$

The line $(\frac{1}{2}q)K = \Delta$ corresponds to zero magnetic field in this Ising model, and is closed under our renormalization procedure. The large K (i.e., low temperature) segment of this line is a first-order boundary between $\langle t_i \rangle \gtrless \frac{1}{2}$ phases. Initial conditions on this segment flow, under successive renormalizations, to the fixed point (2.33). The small K (high temperature) segment forms part of a smooth trend (no phase transition) across $\langle t_i \rangle = \frac{1}{2}$, and flows to a high-temperature fixed point at $V(\theta) = K = \Delta = 0$. The low- and high-temperature segments are separated by the critical fixed point (C in Fig. 9) at

$$V(\theta) = 0, \quad K_c^* = 1.2188, \quad \Delta_c^* = (\tfrac{1}{2}q)K_c^* \tag{2.36}$$

Within our approximate treatment, unstable (relevant) deviations from this fixed point have the eigenvalue exponents $\lambda_H = 1.797$ for the magnetic field direction and $\lambda_T = 0.747$ for the thermal direction. These numbers are to be compared with the exact results [31]

$$K_c = \ln 3 = 1.0986, \quad \lambda_H = \tfrac{15}{8} = 1.875, \quad \text{and} \quad \lambda_T = 1 \ .$$

E. Global Hamiltonian flows

The global Hamiltonian flows, which connect the special limits of Sec. II C and II D, are given schematically in Fig. 9. In this figure, the axis parameter

$$J_{\text{eff}} \equiv -\frac{d^2V(\theta)}{d\theta^2}\Big|_{\theta=0} \ , \tag{2.37}$$

introduced in Ref. 22, measures the coupling between the XY degrees of freedom. It equals J for the initial cosine potential (2.2), and it is approximately (sums replaced by integrals) J_v for the Villain potential (2.25). The choice of the other axis parameter,

$$D \equiv (\Delta + \ln A_4)/K \ , \tag{2.38}$$

is motivated by the asymptotic first-order conditions (2.31c) and (2.33c).

In Fig. 9, the domain of attraction C_0C of the Ising-critical fixed-point C [Eq. (2.36)] terminates the first-order domains of the fixed-line segment F_0F_1 [Eq. (2.31)] and of the fixed-point F [Eq. (2.33)]. Within these combined first-order domains, F_0F_1 (F) is the terminus of flows from regions of strong (weak) XY coupling J_{eff}.

The fixed-line segment S_0S_1 [Eq. (2.26)] of the pure XY model is the sink for the superfluid region of the dilute system. This superfluid region is at small J_{eff}^{-1}, and to the left of the figure. It is bounded by two surfaces: (i) Flows terminating along the whole length of F_0F_1. These flows constitute a boundary of first-order phase transitions. (ii) Flows terminating at S_1, the edge of the fixed-line segment. Separating $\Delta \to -\infty$ limits of opposite stability (Sec. II C), these flows are a renormalization-group separatrix. They constitute a boundary of higher-order phase transitions, of the same type as in the pure XY model. Since Δ is marginal [Eq. (2.30)] at S_1, the correlation-length critical exponent is

$$\nu = \infty \ . \tag{2.39}$$

The higher-order boundary mentioned above terminates on the first-order domains in a line EF_1 of critical end points, between the domains of F_0F_1 and F. Although for small K/J_{eff} the line EF_1 of end-points comes very close to the Ising-critical line C_0C, there is always a strip in between them which flows to the

Ising first-order fixed-point F. Unlike the renormalization-group treatments[9–11] of the discrete BEG model,[1] no tricritical fixed point occurs.

Finally, not shown in Fig. 9, a "paramagnetic" fixed line at $V(\theta)=K=0$, Δ arbitrary, is the sink for the normal-fluid regions.

III. PHASE DIAGRAMS AND SUPERFLUID DENSITY

Phase diagrams result from applying the renormalization procedure to the initial vectorialized BEG Hamiltonian (1.2a). The ratio K/J is associated with fixed experimental conditions, such as film thickness and substrate type. Thus, temperature (J^{-1}) and chemical potential are to be scanned for fixed K/J.

Typical phase diagrams are given in Figs. 7 and 8 in the temperature-chemical potential variables, and, correspondingly, in Figs. 2 and 3 in the temperature-concentration variables. The chemical potential variable D, which has spin-wave corrections to asymptotic first-order behavior subtracted [Eqs. (2.31c) and (2.38)], has been used. Thus, the phase diagrams in thermodynamic field space (Figs. 7 and 8) are quite similar to the ones obtained for the discrete BEG model.[1–3,6,8–11] Operationally, the temperature-chemical potential phase boundaries are determined first. Evaluating concentrations at these boundaries yields the temperature-concentration phase diagram. The chain-rule method,[30] rather than the numerical differentiation of the free energy, was used in calculating concentrations. Trajectories flowing onto the superfluid sink (2.26) were in general stopped after thirty iterations, unless more iterations were needed for convergence.

Figures 2 and 7 show distinctly end-point[9] phase diagrams for $K/J=1$. First-order phase transitions separate ^{4}He-rich and ^{3}He-rich fluids. The ^{4}He-rich fluid undergoes the superfluid transition. Inside the superfluid phase, the numbered curves are lines of constant ρ_s/k_BT (Sec. II B). Thus, the curve numbered n corresponds to $\rho_s/k_BT=16\,m^2/n\pi\hbar^2$. Curve $n=8$, $\rho_s/k_BT=2\,m^2/\pi\hbar^2$, is the superfluid transition line. It terminates at the critical end-point E (Fig. 7) on the first-order boundary, at a temperature J_E^{-1} distinctly lower than the phase-separation critical temperature J_c^{-1}. No multicritical phenomena occur. In the temperature-concentration diagram of Fig. 2(a), the two-phase coexistence regions are inside the dashed boundary. In these regions, the ^{4}He-rich domains undergo the superfluid transition at the end-point temperature J_E^{-1}. Note the minute region occupied by the single (nonseparated) superfluid phase in this diagram. [This region is shown with smaller concentration scale in Fig. 2(b).] For increasing K/J values, C moves to higher J^{-1}, E_4 moves closer to $x=0$, and phase separation masks single superfluidity more and more.

Figures 3 and 8 are for $K/J=0$, the Blume-Capel[2] plane. If the results for $K/J=0$ were viewed with a fine enough resolution, the situation would be qualitatively identical to the case of $K/J=1$, discussed in the preceding paragraph. However, Figs. 3(a) and 8(a) are drawn with the same scales as the corresponding Figs. 2(a) and 7, and the quantitative difference is obvious. Indeed, as K/J is decreased from 1, the superfluidity end-point E and the phase-separation critical point C approach each other, but never actually meet. For $K/J=0$, these points occur at temperatures $J_E^{-1}=0.6581$ and $J_c^{-1}=0.6615$. The corresponding concentrations are

$$x(E_4)=0.12\,,\quad x(C)=0.16\,,\quad \text{and } x(E_3)=0.27\,.$$

The phase diagrams of Figs. 3(a) and 8(a), at these scales, seemingly exhibit tricritical topologies.[1–3,6,8–11,30] In Fig. 8(a), lines of constant ρ_s/k_BT apparently converge onto an "effective" tricritical point T_e, in agreement with the prediction of tricritical scaling theory (Sec. II B). Curves 8 through 5 have $\rho_s/k_BT=2\,m^2/\pi\hbar^2$ through $(3.2)\,m^2/\pi\hbar^2$. However, Fig. 8(b) details the region in which the higher- and first-order boundaries come together. [In going from Fig. 8(a) to 8(b), the horizontal and vertical scales were blown up by factors of 333 and 125, respectively. Thus, Fig. 8(b) actually covers less area than the black point at T_e in Fig. 8(a)]. The end-point structure is seen in Fig. 8(b). Similarly, although the apparent portioning of the $K/J=0$ phase diagram in Fig. 3(a) evokes tricriticality, note the shape of the phase-separation boundary. The same flatness exists, at the top, as for $K/J=1$ in Fig. 2(a). In fact, the neighborhood of point C in both cases originates renormalization-group trajectories which are explicitly traced to the Ising-critical fixed point (2.36). Accordingly, as the critical temperature is approached from below, the coexisting ^{3}He concentrations should merge with the Ising exponent $\beta=\frac{1}{8}$, as in Eq. (1.11). Finally, $x(E_4)=0.12$ is the maximum amount of ^{3}He which can be included into a superfluid domain. The difference from the upper-limit $x=0.67$ of bulk systems[32] is rationalized on dimensional grounds in Sec. I.

Of experimental interest are the superfluid densities ρ_s. (We refer to *areal* densities in the remainder of this section.) Equations (1.4) and (2.19) give

$$\rho_s/\rho_0=J_v/J \tag{3.1a}$$

within the superfluid phase. Here, ρ_0 is the bare superfluid density, which, for a given coverage, could be approximated by $\rho_s(T=0,\,x=0)$. J_v is the Villain interaction[42] on the superfluid sink (2.26) to which the Hamiltonian (1.2a) is renormalized. Furthermore we have

$$\frac{\rho_s}{\rho_0} = \frac{J_v}{J}\frac{x_+ - x}{x_+ - x_-} \tag{3.1b}$$

within the region of coexisting superfluid and normal fluid. Here $x_\pm$ are the coexisting ^{3}He concentrations, and J_v is the Villain interaction on the first-order fixed line (2.31) to which Eq. (1.2a) is renormalized. The crossover between the two fixed lines is such that no discontinuity in the magnitude of ρ_s/ρ_0 occurs at the boundary between Eqs. (3.1a) and (3.1b). We note that in experiments probing superflow in very thin films, Eq. (3.1b) may not be detected at large x due to the complete isolation of superfluid domains.[13] This percolative "shorting" of the superflow should not occur in thicker films or on uniform substrates.

Equations (3.1) were used to determine the superfluid density fraction ρ_s/ρ_0 as a function of temperature (J^{-1}) at fixed concentration. Four types of curves are encountered, as displayed in Fig. 4 for $K/J=0$.

(i) At zero ^{3}He concentration x, ρ_s/ρ_0 jumps from zero to $(2/\pi)J^{-1}$ as predicted by the universal superfluid transition.[23] As temperature is lowered, $(\rho_s/\rho_0)_{x=0}$ in Fig. 4 gradually goes to unity, much like the experimental curves.[25]

(ii) The addition of any ^{3}He brings about a new feature: a kink (slope discontinuity) in the ρ_s/ρ_0 curve, labeled P in Fig. 4. This marks the phase separation at a temperature below the superfluid transition. The latter is still universal, with $(\rho_s/\rho_0)_{\min} = (2/\pi)J^{-1}$. The kink in the ρ_s/ρ_0 curve moves from zero temperature to the superfluid transition temperature as x is changed from zero to $x(E_4)$.

(iii) Between the end-point concentrations $x(E_4)$ and $x(E_3)$, as the system is cooled, phase separation occurs before superfluidity. Then, the ^{4}He-rich domains undergo the superfluid transition at the end-point temperature J_E^{-1}. The transition discontinuity in ρ_s/ρ_0 decreases linearly with x, from its universal value $(2/\pi)J_E^{-1}$ at $x(E_4)$ to zero at $x(E_3)$.

(iv) In the final regime, $x > x(E_3)$, superfluidity appears with phase separation, which is into a ^{4}He-rich superfluid and a ^{3}He-rich normal fluid. The density fraction ρ_s/ρ_0 rises from zero linearly in temperature. This superfluid transition driven by phase separation occurs at a temperature which decreases from J_E^{-1} to zero, as x is changed from $x(E_3)$ to unity.

As seen in Fig. 4, the locus of minimum superfluidity is the universally sloped line

$$(\rho_s/\rho_0)_{\min} = (2/\pi)J^{-1} \quad \text{for } 0 \leq x \leq x(E_4) \ ,$$

the vertical line at J_E^{-1} for $x(E_4) \leq x \leq x(E_3)$, and finally the no-jump situation

$$(\rho_s/\rho_0)_{\min} = 0 \quad \text{for } x(E_3) \leq x \leq 1 \ .$$

For $K/J=0$, the transition discontinuity of ρ_s disappears within the relatively small concentration interval $0.12 < x < 0.27$. In the case of a hypothetical tricritical point, this interval would have shrunk to zero, yielding the indeterminacy of the superfluid density predicted by tricritical scaling (Sec. II B).

Note added in proof: An n-component generalization of the BEG model has been solved exactly for $n \to \infty$ by V. J. Emery, Phys. Rev. B 11, 3397 (1975). In this system, a critical end point occurs instead of a tricritical point, in less than three dimensions. Thus, there seems to be a line in n, d space marking the disappearance of tricriticality. This is in agreement with $d = 3 - \epsilon$ expansion work by M. J. Stephen and J. L. McCauley, Jr., Phys. Lett. A 44, 89 (1973), and unpublished work by these authors. This line passes between $d=2$ and 3 at $n=2$ if our present result is correct, and joins $d=3$ at $n=\infty$. We thank V. J. Emery and M. J. Stephen for bringing this point to our attention.

ACKNOWLEDGMENTS

We are grateful to B. I. Halperin, S. Ostlund, J. D. Reppy, and A. P. Young for most useful conversations. This research was in part supported by the NSF under Grant No. DMR77-10210. One of us (A.N.B.) was supported in part by an IBM Postdoctoral Fellowship. D.R.N. was supported in part by a Junior Fellowship from the Harvard Society of Fellows. After this work was completed, we learned that J. L. Cardy and D. J. Scalapino had performed similar calculations, but on a square instead of triangular lattice.

APPENDIX: VORTEX SPECIFIC HEAT

Here, we present an approximate evaluation of the specific heat in the $\Delta \to -\infty$ limit of the generalized BEG model. According to Kosterlitz and Thouless,[18,21] the partition function of a pure XY model should factor approximately into a spin-wave part, and a set of interacting vortices. This factorization is exact for the Villain model discussed in Sec. II. For more general XY models we expect that such a factorization holds approximately out to, say, twice the transition temperature T_s. We shall concentrate on the vortex part of the specific heat, since the spin waves make only a small constant contribution. This background spin-wave specific heat is, in any case, incorrect at low temperatures due to quantum effects.

Vortex excitations are controlled by the Coulomb

Hamiltonian,[21]

$$-\frac{\mathcal{H}^V}{k_B T}=\pi J \sum_{\vec{r}\neq\vec{r}'} m(\vec{r})m(\vec{r}')\ln(|\vec{r}-\vec{r}'|) - \ln y \sum_{\vec{r}} m^2(\vec{r}) \ , \quad \text{(A.1)}$$

where J and $\ln y$ are respectively the nearest-neighbor interaction energy and the vortex-core energy, both divided by $-k_B T$, and $m(\vec{r})=0, \pm 1, \pm 2, \ldots$, is the vortex charge. The vortex excitations occur on, say, a square lattice of sites with unit spacing, which we also take as the core diameter. The core energy is temperature independent at low temperatures, and proportional[21] to $k_B TJ$. Our aim here is to evaluate the reduced free energy

$$\bar{\mathcal{F}} \equiv \frac{-\mathcal{F}}{k_B T} = \ln Z \ , \quad \text{(A.2)}$$

where

$$Z = \sum_{\{m(\vec{r})\}}{}' e^{-\mathcal{H}^V/k_B T} \ . \quad \text{(A.3)}$$

The prime restricts the summation to those complexions of charges which satisfy $\sum_{\vec{r}} m(\vec{r})=0$. The specific heat can then be determined from

$$C = k_B \frac{d}{dT}\left(T^2 \frac{d}{dT}\bar{\mathcal{F}}\right) \ . \quad \text{(A.4)}$$

A direct evaluation of Eq. (A.3) can be difficult, especially near the transition point. The free energy near T_s is related, however, to this same quantity evaluated at transformed couplings by renormalization-group recursion relations. A renormalization transformation which scales up the core diameter from 1 to e^l leads to a Hamiltonian with parameters $J(l)$ and $y(l)$ which satisfy

$$\frac{dJ^{-1}(l)}{dl} = 4\pi^3 y^2(l) \ , \quad \text{(A.5a)}$$

$$\frac{d\,y(l)}{dl} = [2-\pi J(l)]y(l) \ . \quad \text{(A.5b)}$$

These equations, correct to $O(y^2)$, must be supplemented by an equation for the way in which the free energy transforms, namely,[46]

$$\bar{\mathcal{F}}\{J(0),y(0)\} = 2\pi \int_0^l e^{-2l'} y^2(l')\,dl' + e^{-2l}\bar{\mathcal{F}}\{J(l),y(l)\} \ . \quad \text{(A.6)}$$

The familiar Hamiltonian flows induced by Eq. (A.5) are shown schematically in Fig. 10. The locus of initial conditions corresponding to $\ln y \sim -J$ is shown as a dashed line. Below T_s (i.e., to the left of the incoming separatrix), $y(l)$ is initially small and tends to zero. Equation (A.6) can then be evaluated

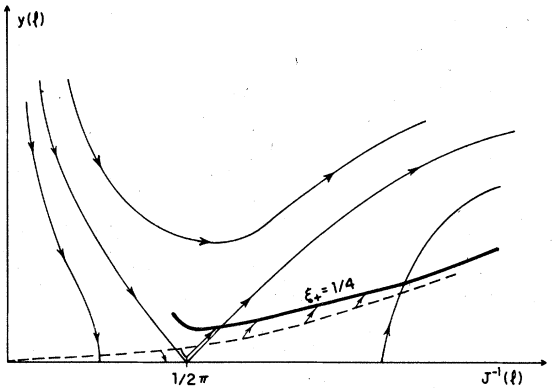

FIG. 10. Hamiltonian flows for the two-dimensional XY model without impurities. The low-temperature phase is the domain of attraction of the fixed line at $y(l)=0$. The dashed line is the locus of initial conditions, and the heavy line is the locus $\xi_+=\frac{1}{4}$ in the high-temperature phase. The transition temperature is given by the intersection of the dashed line and the incoming separatrix. At temperatures, say, 10% or more above T_s, the line $\xi_+=\frac{1}{4}$ should be given to a good approximation by Eq. (A.9). The free energy can be calculated above T_s by integrating Hamiltonians until they reach the line $\xi_+=\frac{1}{4}$, and then using Debye-Hückel theory.

in the limit $l\to\infty$, i.e.,

$$\bar{\mathcal{F}}\{J(0),y(0)\} = 2\pi \int_0^\infty e^{-2l'} y^2(l')\,dl' \quad (T<T_s) \ . \quad \text{(A.7)}$$

Above T_s, $y(l)$ eventually increases, and begins to move outside the domain of validity of Eqs. (A.5). Progress can be made, however, by stopping the flows before $y(l)$ becomes too large. One can then determine the free energy on the right-hand side of Eq. (A.6) using Debye-Hückel theory, which should be correct at sufficiently high temperatures.

Debye-Hückel theory amounts to replacing the sums over vortex charges in Eq. (A.3) by integrals. Upon Fourier transformation, $\mathcal{H}^V$ then becomes

$$\frac{\mathcal{H}^V}{k_B T} = \frac{1}{8\pi^2}\int d^2k \left(\frac{A}{k^2}+B+O(k^4)\right) m(\vec{k})m(-\vec{k}) \ , \quad \text{(A.8a)}$$

where

$$m(\vec{k}) = \sum_{\vec{r}} e^{i\vec{k}\cdot\vec{r}} m(\vec{r}) \ , \quad \text{(A.8b)}$$

and

$$A = 4\pi^2 J \ , \quad B = -8\pi(\ln y + \pi J c) \ . \quad \text{(A.8c)}$$

The quantity c is a cutoff dependent constant which is[21] approximately equal to $\frac{1}{2}\pi$ for a square lattice. We have used a small k approximation for the Fourier-transformed potential, and will, for convenience, restrict the k integrations to a circular Brillouin zone of unit radius. Above T_s, correlations are expected to decay exponentially. It is straightforward to check that Eqs. (A.8) do indeed lead to exponentially decaying correlations, with correlation length

$$\xi_+^2 \approx B/A \quad . \tag{A.9}$$

One expects this formula to hold only at temperatures at least, say, 10% above T_s, where the physics is dominated by Debye-Hückel screening.

To determine the free energy above T_s, we evaluated Eq. (A.6) with $\ln y = 5.2\,J$. The proportionality constant 5.2 was chosen to insure that B in Eq. (A.8c) is positive for $c = \frac{1}{2}\pi$. Otherwise, higher-order terms in k^2 in Eq. (A.8a) would have to be included to obtain sensible results. The recursion relations were integrated numerically until we had $l = l^*$ such that ξ_+ was $\frac{1}{4}$, as given by the Debye-Hückel approximation. The value $\xi_+ = \frac{1}{4}$ was chosen for convenience; any number of order unity would do. At this point, we estimated $\bar{\mathfrak{F}}\{J(l^*), y(l^*)\}$ using Eq. (A.8a), i.e.,

$$\bar{\mathfrak{F}}\{J(l^*), y(l^*)\} \approx \frac{1}{4\pi}\int_0^1 \ln\left[\frac{A(l^*)}{k^2} + B(l^*)\right] k\, dk \quad , \tag{A.10}$$

where $A(l)$ and $B(l)$ are the l-dependent quantities corresponding to Eq. (A.8c). Equation (A.7) was evaluated numerically to obtain $\bar{\mathfrak{F}}$ below T_s.

The specific heat derived from differentiating this free energy is shown in Fig. 5. It rises exponentially from zero, passes smoothly through T_s, and reaches a maximum about 38% above the critical temperature. The maximum is caused by a dissociation of vortices with smaller and smaller separation with increasing temperatures. At sufficiently high temperatures, essentially all vortices are unbound, and the specific heat drops.

The specific heat could also be computed directly from Migdal's renormalization procedure, as has been done by Kirkpatrick.[47] Figure 5 resembles Kirkpatrick's curves, provided a constant spin-wave contribution is added. The present result (Fig. 5) derives from a theory with a genuine finite-temperature phase transition.

[1] M. Blume, V. J. Emery, and R. B. Griffiths, Phys. Rev. A 4, 1071 (1971).

[2] Earlier treatments of Hamiltonian (1.1) with no biquadratic interaction ($K = 0$) are M. Blume, Phys. Rev. 141, 517 (1966); H. W. Capel, Physica (Utrecht) 32, 966 (1966); 33, 295 (1967); 37, 423 (1967).

[3] D. Mukamel and M. Blume, Phys. Rev. A 10, 610 (1974); J. Lajzerowicz and J. Sivardière, *ibid.* 11, 2079 (1975); J. Sivardière and J. Lajzerowics, *ibid.* 11, 2090 (1975); 11, 2101 (1975); D. Furman, S. Dattagupta, and R. B. Griffiths, Phys. Rev. B 15, 441 (1977).

[4] E. K. Riedel and F. J. Wegner, Phys. Rev. Lett. 29, 349 (1972).

[5] F. J. Wegner and E. K. Riedel, Phys. Rev. B 7, 248 (1973).

[6] D. M. Saul, M. Wortis, and D. Stauffer, Phys. Rev. B 9, 4964 (1974).

[7] P. C. Hohenberg, Phys. Rev. 158, 383 (1967); N. D. Mermin, J. Math. Phys. 8, 1061 (1967).

[8] B. L. Arora and D. P. Landau, AIP Conf. Proc. 10, 870 (1973).

[9] A. N. Berker and M. Wortis, Phys. Rev. B 14, 4946 (1976).

[10] T. W. Burkhardt, Phys. Rev. B 14, 1196 (1976); T. W. Burkhardt, H. J. F. Knops, and M. den Nijs, J. Phys. A 9, L179 (1976).

[11] J. Adler, A. Aharony, and J. Oitmaa, J. Phys. A 11, 963 (1978).

[12] P. C. Hohenberg, in *Proceedings of the Enrico Fermi Summer School of Physics,* edited by M. S. Green (Academic, New York, 1971).

[13] Superfluidity in the presence of phase separation has been considered by J. G. Dash, Phys. Rev. Lett. 41, 1178 (1978).

[14] F. J. Wegner, Z. Phys. 206, 465 (1967).

[15] H. E. Stanley, Phys. Rev. Lett. 20, 150 (1968); 20, 589 (1968). Also see M. A. Moore, *ibid.* 23, 861 (1969); W. J. Camp and J. P. Van Dyke, J. Phys. C 8, 336 (1975).

[16] N. D. Mermin and H. Wagner, Phys. Rev. Lett. 17, 1133 (1966).

[17] V. L. Berezinskii, Zh. Eksp. Teor. Fiz. 59, 907 (1970) [Sov. Phys. JETP 32, 493 (1971)].

[18] J. M. Kosterlitz and D. J. Thouless, J. Phys. C 6, 1181 (1973).

[19] J. Zittartz, Z. Phys. B 23, 55 (1976); 23, 63 (1976).

[20] A. Luther and D. J. Scalapino, Phys. Rev. B 16, 1153 (1977).

[21] J. M. Kosterlitz, J. Phys. C 7, 1046 (1974).

[22] J. V. José, L. P. Kadanoff, S. Kirkpatrick, and D. R. Nelson, Phys. Rev. B 16, 1217 (1977).

[23] D. R. Nelson and J. M. Kosterlitz, Phys. Rev. Lett. 39, 1201 (1977).

[24] I. Rudnick, Phys. Rev. Lett. 40, 1454 (1978).

[25] D. J. Bishop and J. D. Reppy, Phys. Rev. Lett. 40, 1727 (1978).

[26] Experimental results for films of ^{3}He-^{4}He mixtures are in (a) B. Ratnam and J. Mochel, in *Low Temperature Physics-LT13,* edited by K. D. Timmerhaus, W. J. Sullivan, and E. F. Hammel (Plenum, New York, 1974), Vol. 1; (b) E. Webster, G. Webster, and M. Chester (unpublished).

[27] A. A. Migdal, Zh. Eksp. Teor. Fiz. 69, 1457 (1975) [Sov. Phys. JETP 42, 743 (1976)].

[28] L. P. Kadanoff, Ann. Phys. (New York) 100, 359 (1976); Rev. Mod. Phys. 49, 267 (1977).

[29] Another type of phase diagram, intermediate to the two discussed here, involves a tricritical point and a triple

point (Refs. 1, 3, and 9). In still another possibility [J. M. Kincaid and E. G. D. Cohen, Phys. Lett. A 50, 317 (1974)], the transition line from the pure system stretches over the tip of the coexistence curve and joins this curve on the very diluted side.

[30]A. N. Berker, S. Ostlund, and F. A. Putnam, Phys. Rev. B 17, 3650 (1978).

[31]L. Onsager, Phys. Rev. 65, 117 (1944); C. N. Yang, *ibid.* 85, 809 (1952); R. M. F. Houtappel, Physica (Utrecht) 16, 425 (1950).

[32]E. H. Graf, D. M. Lee, and J. D. Reppy, Phys. Rev. Lett. 19, 417 (1967). For general reviews, see (a) G. Ahlers, in *The Physics of Liquid and Solid Helium, Part I,* edited by K. H. Benneman and J. B. Ketterson (Wiley, New York, 1976); (b) C. Ebner and D. O. Edwards, Phys. Repts. C 2, 77 (1971).

[33]M. A. Eggington and M. A. Moore, J. Low Temp. Phys. 15, 99 (1974).

[34]Stacked two-dimensional Ising models were studied by J. Oitmaa and I. G. Enting, J. Phys. A 8, 1097 (1975); S. E. Ashley and M. B. Green, J. Phys. A 9, L165 (1976); M. J. De Oliveira and R. B. Griffiths, Surf. Sci. 71, 687 (1978). The latter work also introduced the vertically varying chemical potential.

[35]L. P. Kadanoff, Phys. Rev. Lett. 34, 1005 (1975); L. P. Kadanoff, A. Houghton, and M. C. Yalabık, J. Stat. Phys. 14, 171 (1976).

[36]V. J. Emery and R. H. Swendsen, Phys. Lett. A 64, 325 (1977); Phys. Rev. Lett. 39, 1414 (1977).

[37]B. D. Josephson, Phys. Lett. 21, 608 (1966).

[38]P. C. Hohenberg, A. Aharony, B. I. Halperin, and E. D. Siggia, Phys. Rev. B 13, 2986 (1976).

[39]J. Rudnick and D. Jasnow, Phys. Rev. B 16, 2032 (1977).

[40]P. C. Hohenberg and P. C. Martin, Ann. Phys.(Paris) 34, 291 (1965).

[41]B. I. Halperin and P. C. Hohenberg, Phys. Rev. 188, 898 (1969).

[42]J. Villain, J. Phys. (Paris) 36, 581 (1975).

[43]E. K. Riedel, Phys. Rev. Lett. 28, 675 (1972).

[44]M. Nauenberg and B. Nienhuis, Phys. Rev. Lett. 33, 1598 (1974); B. Nienhuis and M. Nauenberg, Phys. Rev. B 11, 4153 (1975).

[45]R. B. Griffiths, Physica (Utrecht) 33, 689 (1967).

[46]J. M. Kosterlitz, J. Phys. C 10, 3753 (1977).

[47]S. Kirkpatrick (private communication).